Nanostructured High-Energy $xLi_2MnO_3\cdot(1\text{-}x)LiNi_{0.5}Mn_{0.5}O_2$ $(0.3 \leq x \leq 0.6)$ Cathode Materials

Xiaofeng Zhang, Miklos Lengyel, and Richard L. Axelbaum
Dept. of Energy, Environmental and Chemical Engineering, Washington University in St. Louis, St. Louis, MO 63130

DOI 10.1002/aic.14287
Published online December 19, 2013 in Wiley Online Library (wileyonlinelibrary.com)

Nanostructured lithium-manganese-rich nickel-manganese-oxide $xLi_2MnO_3\cdot(1\text{-}x)LiNi_{0.5}Mn_{0.5}O_2$ *(*$0.3 \leq x \leq 0.6$*) composite materials were synthesized via spray pyrolysis using mixed nitrate precursors. All the materials showed a composite structure consisting of* Li_2MnO_3 (C2/m) *and* $LiNi_{0.5}Mn_{0.5}O_2$ ($R\bar{3}m$) *components, and the amount of* Li_2MnO_3*-phase appeared to increase with* x*, as observed from XRD analysis. These composite materials showed a high-discharge capacity of about 250* $mAhg^{-1}$*. In the range of* x *considered, the layered* $0.5Li_2MnO_3\cdot0.5LiNi_{0.5}Mn_{0.5}O_2$ *materials displayed the highest capacity and superior cycle stability. Nonetheless, voltage suppression from a layered-spinel phase transition was observed for all the composites produced. This voltage suppression was dependent of the amount of* Li_2MnO_3 *phase present in the composite structure.* © 2013 American Institute of Chemical Engineers *AIChE J*, 60: 443–450, 2014

Keywords: Li-Mn-rich cathode, $xLi_2MnO_3\cdot(1\text{-}x)LiNi_{0.5}Mn_{0.5}O_2$*, spray pyrolysis, high-energy, Li-ion battery*

Introduction

Li-ion batteries (LIBs) are becoming attractive and popular means of energy storage for the transportation sector, due to their high-energy densities.[1,2] A LIB cell consists of an anode and a cathode, which are normally soaked in an electrolyte, and separated by an electronically nonconductive membrane. The anode typically consists of graphite-based materials. The cathode materials are typically lithium metal oxides with layered, spinel or a polyanion structure.[1,2] Of particular interest in this article are the layered materials, as one Li per transition metal is intercalatable in $LiMO_2$ (where M = Ni, Mn, Co), allowing these materials to achieve a high-energy density. The commercialized $LiCoO_2$ is isostructural to α-$NaFeO_2$ ($R\bar{3}m$ symmetry) with the oxygen atoms in a cubic-close-packed (*ccp*) arrangement, and this material displays a good capacity and cycleability.[3,4] However, the cost of Co is high and the thermal runaway of the $LiCoO_2$ cell can be a safety concern for consumers.[5] Alternatively, various layered Ni-based or Mn-based lithium metal oxides have been developed to replace the Co-based materials.[5–8] Unfortunately, stoichiometric $LiNiO_2$ materials encounter challenges for synthesis due to the disordering of the Li and Ni ions in the 3(a) and 3(b) sites, respectively, and this deteriorates battery performance.[6] The thermodynamically stable $LiMnO_2$ has an orthorhombic structure (*Pmnm* symmetry), but can convert to spinel structure over extensive cycles, yielding poor cycle stability.[3,4,9,10] Many optimization studies of synthetic routes and material chemistry have been conducted to overcome the negative aspects of these materials,[7,11] and the family of layered Li-Mn-rich nickel-manganese-cobalt metal oxides (LMR—NMC) is one of the most attractive candidates.[12–18]

LMR—NMC composites have achieved capacities of more than 250 $mAhg^{-1}$ while maintaining a good structural stability.[12–15] Recent studies have indicated that the LMR—NMC materials can be considered to be integrated composite of two layer-structured materials: monoclinic Li_2MnO_3 (C2/m) and trigonal $LiMO_2$ ($R\bar{3}m$, M = Ni, Mn, and/or Co).[15,19] The closed-packed oxygen layers in these two structures are compatible, and, therefore, can integrate at the atomic level.[19,20] Consequently, the integrated layered-layered composites can be written as $xLi_2MnO_3\cdot(1\text{-}x)LiNi_\alpha Mn_\beta Co_{(1-\alpha-\beta)}O_2$ (where $0 < x < 1$). Monoclinic Li_2MnO_3 alone is normally considered to be electrochemically inactive, where the tetravalent Mn cannot be oxidized upon delithiation within the normal operation voltage window (lower than 5 V vs. Li/Li^+). However, in the composites, the Li_2MnO_3 component not only works as a structural stabilizing agent, but most importantly can provide anomalous capacities (over 250 $mAhg^{-1}$) after its electrochemical activation above ca. 4.5 V (vs. Li/Li^+).[15,21–24]

Nonetheless, at the early stage of the development of these materials, a high capacity over 200 $mAhg^{-1}$ could only be achieved at very low-current densities (C/20 $\sim$ C/50) for bulk materials.[12–15] Fortunately, by reducing the primary particle size and increasing the porosity of the secondary particles, these composite materials can achieve significantly higher rate capabilities, making them more suitable for PHEV (plug-in hybrid electric vehicle) applications.[25–27]

Current address of X. Zhang: Chemical Sciences and Engineering Division, Argonne National Laboratory, Argonne, IL 60439
Correspondence concerning this article should be addressed to R. L. Axelbaum at axelbaum@wustl.edu.

Table 1. ICP-MS Analysis of $xLi_2MnO_3\cdot(1\text{-}x)LiNi_{0.5}Mn_{0.5}O_2$ Precursor Solutions

Li_2MnO_3	$LiMn_{0.5}Ni_{0.5}O_2$	Target stoichiometry			As-measured by ICP-MS		
x	(1-x)	Li	Ni	Mn	Li	Ni	Mn
0.3	0.7	1.13	0.30	0.57	1.09	0.28	0.52
0.4	0.6	1.17	0.25	0.58	1.13	0.25	0.55
0.5	0.5	1.20	0.20	0.60	1.21	0.20	0.60
0.6	0.4	1.23	0.15	0.62	1.34	0.16	0.64

Herein, we explore how the Li_2MnO_3 content affects the overall performance of the Co-free LMR—NMC materials synthesized via spray pyrolysis. Spray pyrolysis can precisely control the particle-size distribution, elemental composition, purity and uniformity of the final product; therefore, it has been explored extensively in the synthesis of nanostructured single-phased transition metal oxides and phosphates, e.g., $LiMn_2O_4$, $Li[Ni_{1/3}Co_{1/3}Mn_{1/3}]O_2$, $LiNi_{0.5}Mn_{1.5}O_4$ and $LiFePO_4$ for Li-ion batteries.[28–37] Recently, spray pyrolysis has drawn attentions in the composite cathode materials synthesis, which gave outstanding performance.[27,38–40] For ease, we adopt the composite formula $xLi_2MnO_3\cdot(1\text{-}x)LiNi_{0.5}Mn_{0.5}O_2$ in this article, which can both reflect the Li-Mn concentration and consequently the amount of Li_2MnO_3 component in the composite structures. Powders with a range of x values are synthesized, and the physical and electrochemical properties of the powders are studied and evaluated.

Experimental

A tubular aerosol flow reactor was used to produce the $xLi_2MnO_3\cdot(1\text{-}x)LiNi_{0.5}Mn_{0.5}O_2$ $(0.3 \le x \le 0.6)$ composite materials.[27] The precursor solution was prepared by dissolving $LiNO_3$, $Mn(NO_3)_2\cdot4H_2O$ and $Ni(NO_3)_2\cdot6H_2O$ in stoichiometric proportions in deionized water. The total molar concentrations of $Mn(NO_3)_2\cdot4H_2O$ and $Ni(NO_3)_2\cdot6H_2O$ were maintained at 2 mol.L^{-1}. The corresponding Li concentration can be calculated based on the x value in the $xLi_2MnO_3\cdot(1\text{-}x)LiNi_{0.5}Mn_{0.5}O_2$ composites. The precursor solution was aerosolized with a one-jet air-assisted nebulizer (Collison, BGI, Inc.), where fine precursor droplets in the micron-size range were produced. After aerosolization, the precursor aerosols were carried by air into a preheater maintained at 250°C (wall temperature), and then a vertical ceramic tube furnace heated to 700°C. Downstream of the reactor, the as-produced powder was collected by a membrane filter (Nuclepore track-etched polycarbonate membrane, pore size: 0.2 μm). The particle-size distribution of the as-synthesized powder was measured with an in-line electric-low-pressure-impactor (ELPI, DEKATI) at the furnace outlet. The as-produced powders were annealed at 800°C for 2 h, followed by slow cooling at 3°C min^{-1}. X-ray powder diffraction data was collected with a Rigaku Diffractometer (Geigerflex D-MAX/A) using Cu-Kα radiation and operated at 35 kV and 35 mA. The scanning range was from 10 to 80° 2θ with a step size of 0.04°s^{-1}. The particle morphology was examined with an FEI Nova 2300 Field Emission scanning electron microscope (SEM). Inductively-coupled-plasma mass spectrometry (ICP-MS, Agilent 7500 ce) was performed to confirm the elemental compositions of the precursor solutions and the powders.

Electrochemical performance of the $xLi_2MnO_3\cdot(1\text{-}x)LiNi_{0.5}Mn_{0.5}O_2$ $(0.3 \le x \le 0.6)$ powders was evaluated with 2032 coin-type half cells (Hohsen Corp.). To prepare the cathode, the active material, polyvinylidene fluoride (PVdF) binder, and Super-P conductive carbon black were blended at a ratio of 80:10:10 by weight, suspended in N-methyl-2-pyrrolidene (NMP) and then homogenized to form a slurry using a Kinematica Polytron homogenizer at a controlled speed. The resulting slurry was cast on aluminum foil using the doctor blade technique to form a uniform thin cathode film. The laminate was dried in a vacuum oven at 130°C overnight, forming a 35 to 50 μm thin film. The cathode was lightly calendered to improve adhesion. Small, round, cathode discs (diameter 13 mm) were punched out of the dry laminate for the 2032 coin-type test cells. A pure lithium foil served as the anode and a 2500 Celgard membrane served as the separator. The electrolyte was 1M $LiPF_6$ in ethylene carbonate/diethyl carbonate/dimethyl carbonate solution (EC:DEC:DMC = 1:1:1 by volume). The coin cells were assembled in a high-purity argon-filled glovebox. All the electrochemical tests were performed at room temperature, 23°C.

Results and Discussion

Elemental and morphology analysis

The compositions of the prepared nitrate precursor solutions were confirmed by ICP-MS before producing powders with the spray pyrolysis system (Table 1). The process temperatures were low (700°C in the reactor and 800°C for post-annealing) and the annealing times were short, suggesting that Li-loss due to evaporation would be negligible. To validate this assumption, the as-produced powder ($x = 0.5$) was digested in concentrated nitric acid and hydrochloric acid solution, and was further diluted to a "ppb" level for ICP-MS analysis. As shown in Table 2, the stoichiometry of the powders before and after annealing was well-preserved. Hence, the synthetic route used in this study to produce the composite materials has advantages over synthesis by co-precipitation. In the latter the Li stoichiometry and consequently the electrochemical properties, are highly dependent on oxidation states of the transition metals in the hydroxide or carbonate precursors (oxidation would occur in air), and the amount of Li loss during the high-temperature calcination process.[41–44] For example, $M(OH)_2$ (where M = Mn, Ni or Co) can be oxidized into transition metal oxides (e.g., Mn_3O_4) or oxyhydroxides (M(OOH)) such that excess Li is often applied during the post-lithiation process to compensate for Li loss due to evaporation.[42–44]

A typical particle-size distribution of the as-synthesized $0.5Li_2MnO_3\cdot0.5LiNi_{0.5}Mn_{0.5}O_2$ powders (secondary particles),

Table 2. ICP-MS Analysis of $xLi_2MnO_3\cdot(1\text{-}x)LiNi_{0.5}Mn_{0.5}O_2$ ($x = 0.5$) Powders Subjected to Different Heat Treatments.

	Normalized Elemental Composition		
Sample	Li	Ni	Mn
Stoichiometric Values	1.20	0.2	0.6
As-synthesized (non-annealed)	1.22	0.2	0.6
800°C for 2 hr	1.24	0.2	0.6
800°C for 10 hr	1.24	0.2	0.6

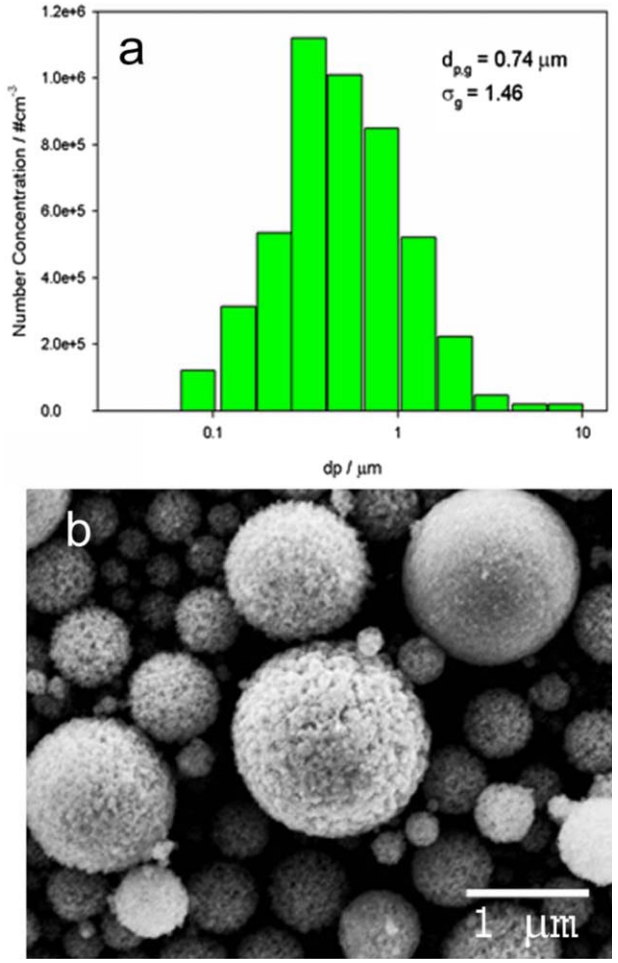

Figure 1. A typical particle-size distribution (a) and SEM photograph of the as-synthesized (nonannealed) xLi$_2$MnO$_3$·(1-x)LiNi$_{0.5}$Mn$_{0.5}$O$_2$ (x = 0.5) composite material (b).

[Color figure can be viewed in the online issue, which is available at wileyonlinelibrary.com.]

as measured by the ELPI, is shown in Figure 1. The particles display a lognormal distribution with a geometric standard derivation of ca. 1.46. The geometric mean diameter of this powder was ca. 0.74 μm. The largest particles measured were about 10 μm in diameter, which is two-orders of magnitude larger than the smallest detected particles (ca. 100 nm). In this regard, the powder is considered poly-dispersed. This particle-size distribution displays the smallest d_{50} reported in the literature for this type of spherical composite materials. Comparing this powder to those from traditional synthesis processes, e.g., coprecipitation, the mean size of the secondary particle from this process is roughly one order of magnitude lower.

The SEM micrographs (Figure 2) indicate that the secondary particles are spherical in shape, highly porous and in the nano- to micron-size range. Moreover, as x increases the primary particle size increases and the surface is coarsened for the same heat treatment. Hence, the ratio of Li_2MnO_3 to $LiNi_{0.5}Mn_{0.5}O_2$, in other words, the Li and Mn content in the composite materials, had a significant effect on the sintering/coarsening process of the powders, and, consequently, the primary particle sizes. This trend was also observed in the synthesis of $Li_{(1+x)}Ni_{0.25}Mn_{0.75}O_{(2.25+x/2)}$ *via* the coprecipitation process, in that a higher Li concentration produced more coarsened secondary particles with larger primary particles under the same heat treatment conditions.[26] It is expected that a higher Li and Mn concentration could reduce the sintering temperature of the composition materials, which facilitates the coarsening of the primary particles.

Crystallographic analysis

The XRD patterns of the as-produced xLi$_2$MnO$_3$·(1-x)LiNi$_{0.5}$Mn$_{0.5}$O$_2$ ($0.3 \leq x \leq 0.6$) powders (collected at the reactor outlet) are shown in Figure 3a. The XRD patterns of the as-produced powders are almost identical. The XRD peaks are very broad due to the ultrafine crystallite size. Nonetheless, these XRD patterns can be indexed to either a rock-salt type layered $LiNiO_2$ ($R\bar{3}m$) or spinel $LiNi_{0.5}Mn_{1.5}O_4$ ($Fd\bar{3}m$) structure. However, the superlattice peaks from the Li_2MnO_3 component are not detectable in the as-produced powder. After annealing at 800°C for 2 h, the materials adopted a rhombohedral $R\bar{3}m$ symmetry, as seen in Figure 3b. All the XRD patterns of these materials show a broad peak between 20 and 25° (2θ), indicating the presence of the Li_2MnO_3-type structure ($C2/m$ symmetry).[25,26] The magnitude of the Li_2MnO_3-type Bragg peaks increases with the amount of Li_2MnO_3 (x value) in the composite materials. Herein, the xLi$_2$MnO$_3$·(1-x)LiNi$_{0.5}$Mn$_{0.5}$O$_2$ is considered a composite material with two compatible layered structures integrated together. The Li_2MnO_3-type structure is expected to be important for maintaining structural stability, and, consequently, the electrochemical properties of the composite material.[15,18,19,45] It also can be seen that the (108) and (110) peaks near 65° (2θ) start to split as the x value increases due to the growing of the parent hexagonal cells with $R\bar{3}m$ space group and formation of a more well-defined layered structure.[16,46]

The Scherrer formula was applied to estimate the average grain size of the as-synthesized and the annealed powders based on the FWHM of the (104) peak near 45° (2θ). These materials are nanometric-grain powders, and after annealing the grain size almost doubles from ca. 10 nm to over 20 nm for all powders (Figure 3c). For the same synthesis and heat-treatment conditions, a linear relationship between grain size and x is also observed, as shown in the supporting materials. Therefore, a high Li_2MnO_3 content or, in another words, a high Li and Mn content facilitates the sintering/coarsening rate of the powders. The increase in the grain size can also lead to an increase in the primary particle size, which is consistent with SEM observations discussed earlier.

Electrochemical performance

Figure 4 shows the initial charge/discharge curves for the Li/xLi$_2$MnO$_3$·(1-x)LiNi$_{0.5}$Mn$_{0.5}$O$_2$ ($0.3 \leq x \leq 0.6$) cells tested at a constant current density of 11.5 mAg^{-1} (equivalent to C/10, 1C = 230 mAg^{-1}) at room temperature. In the first cycle, all four half cells showed a two-step charge profile and a smooth discharge profile between 2.0 and 4.9 V. This voltage shape is consistent with the electrochemical characteristics of xLi$_2$MnO$_3$·(1-x)LiNi$_{0.5}$Mn$_{0.5}$O$_2$.[15,23] In the first cycle, the voltage slowly climbs from 3.5 V to 4.5 V due to the Ni^{2+}/Ni^{4+} redox couple during the extraction of Li.[15,23] At ca. 4.5 V, a voltage plateau appears, which is attributed to the simultaneous removal of Li and O from the Li_2MnO_3 component irreversibly. The net loss in the two-step Li-extraction reactions is believed to be Li_2O from Li_2MnO_3,

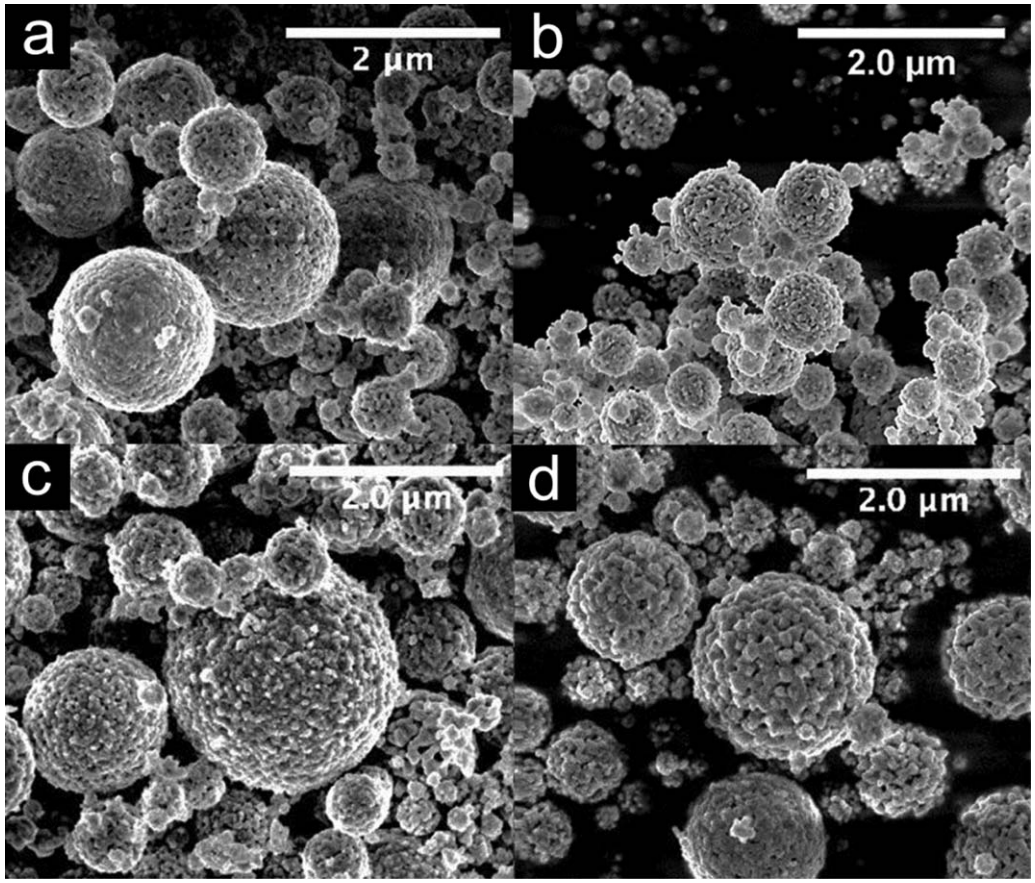

Figure 2. SEM images of the annealed $x\mathrm{Li_2MnO_3}\cdot(1\text{-}x)\mathrm{LiNi_{0.5}Mn_{0.5}O_2}$ ($0.3 \leq x \leq 0.6$) powders synthesized via spray pyrolysis (a) $x = 0.3$, (b) $x = 0.4$, (c) $x = 0.5$, and (d) $x = 0.6$.

after which the electrochemically active MnO_2 component is produced, according to early experimental observations.[15,23] The length of the 4.5 V plateau is elongated with x, and the capacity from the Ni^{2+}/Ni^{4+} redox couple decreases accordingly. It is because the Li_2MnO_3 component increased with x that a longer electrochemical activation is required. During the discharge process, Li can be reinserted into the tetrahedral interstitial sites in MnO_2, forming $LiMnO_2$ (Mn^{4+} to Mn^{3+}). For this reason, the discharge of the $x\mathrm{MnO_2}\cdot(1\text{-}x)\mathrm{Ni_{0.5}Mn_{0.5}O_2}$ electrodes from ca. 4.6 V to 2.0 V is expected to involve three steps: (1) Ni^{4+}/Ni^{3+} redox couple above 3.9 V; (2) Ni^{3+}/Ni^{2+} between 3.9 and 3.5 V, and (3) Mn^{4+}/Mn^{3+} forming $LiMnO_2$ between 3.5 and 2.9 V.[13,15] As the initial activation process involving the oxygen loss reactions in the Li_2MnO_3 component is an irreversible process, the discharge capacity of this type of materials is always noticeably less than the initial charge capacity with a low initial coulombic efficiency.[12,15,27,45] From the discharge profiles, we can also see that the materials with lower x have a higher working potential, which is due to the higher Ni content in these materials.

Nonetheless, the coulombic efficiency of these composites varies with the amount of Li_2MnO_3 in the structure. Assuming that all of the Li is extracted from the Li_2MnO_3 component, the calculated coulombic efficiency would drop linearly with x, because MnO_2 (fully delithiated Li_2MnO_3 product) would take up to one Li per transition metal Mn. Thus, on discharge, half of the Li in Li_2MnO_3 cannot be intercalated reversibly thereafter. The calculated coulombic efficiency for the first cycle is ca. 77% and 62% for $x = 0.3$ and $x = 0.6$, respectively. The composite electrode with $x = 0.5$ attained a coulombic efficiency of ca. 80% in the first cycle, which was the highest among the composite materials in this study. Moreover, the composite with an equal amount of Li_2MnO_3 and $LiNi_{0.5}Mn_{0.5}O_2$ displays the highest discharge capacity (over 270 $mAhg^{-1}$) for the first discharge at the 11.5 mAg^{-1} rate. From this analysis, it can be concluded that the electrochemical performance of these composites cannot be simply considered as a summation of the two individual components and the composite structure may have structural properties that affect the overall battery performance.

Figure 5 shows the cycle performance and corresponding coulombic efficiencies of the $x\mathrm{Li_2MnO_3}\cdot(1\text{-}x)\mathrm{LiNi_{0.5}Mn_{0.5}O_2}$ ($0.3 \leq x \leq 0.6$) half-cells at a current density of 23 mAg^{-1} (C/10 rate) between 2.0 and 4.8 V. For $x \geq 0.5$, the materials have better cycle stability and efficiency (>98.5%) than those for $x < 0.5$ (<98%), possibly due to the presence of high concentrations of the Li_2MnO_3-type component stabilizing the structure.[15,19] Additionally, the primary particle size of the high x material is also higher than that of the others, as observed in the SEM images (Figure 2), thus, the side reactions (dissolution of active species and reactions with the electrolyte) can be minimized. With equal amounts of Li_2MnO_3 and $LiNi_{0.5}Mn_{0.5}O_2$ phases, the composite material yields a superior cycleability and capacity: ca. 225 $mAhg^{-1}$ after 35 cycles. In contrast, the other composite materials ($x = 0.3$, 0.4 and 0.6) can only attain a capacity of ca. 200 $mAhg^{-1}$.

The differential capacity dQ/dV plots of the composite half-cells display a sharp peak above 4.5 V during the first

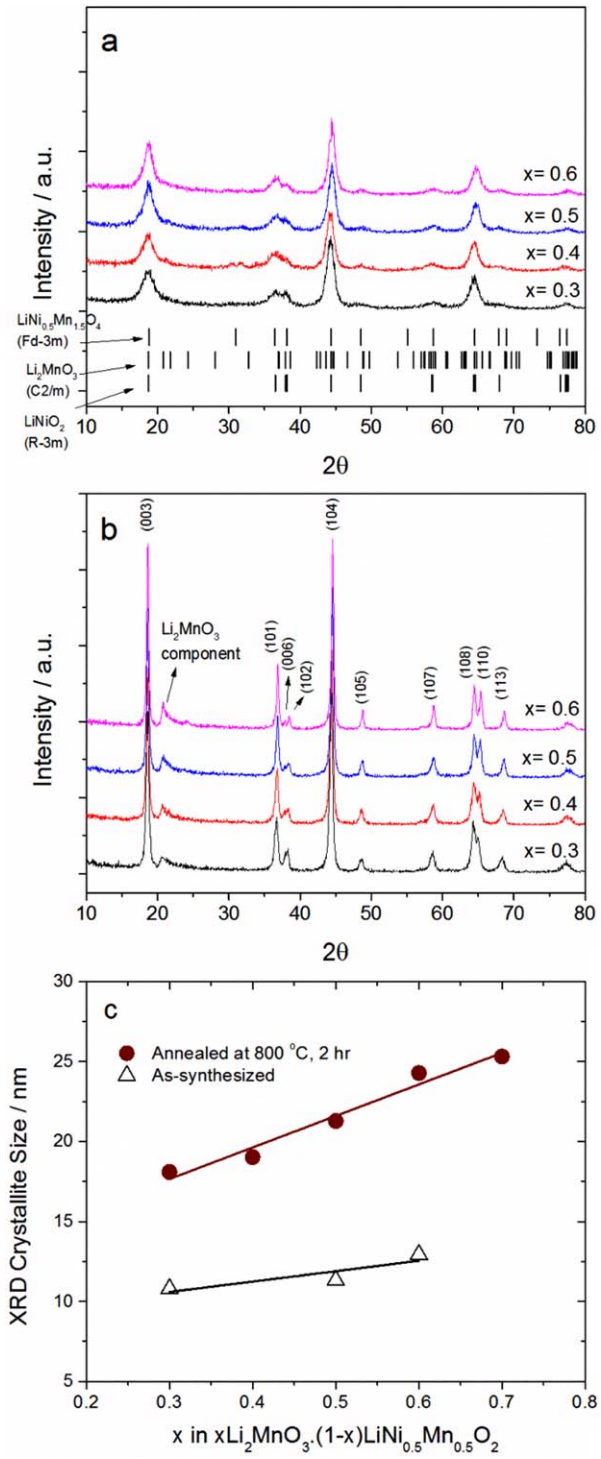

Figure 3. XRD patterns of nanostructured $x\text{Li}_2\text{MnO}_3\cdot(1\text{-}x)\text{LiNi}_{0.5}\text{Mn}_{0.5}\text{O}_2$ $(0.3 \le x \le 0.6)$ powders synthesized via spray pyrolysis (a) as-produced (nonannealed) materials, (b) annealed materials (800°C for 2 h), and (c) average crystallite size calculated by Scherrer formula using the (104) peak.

[Color figure can be viewed in the online issue, which is available at wileyonlinelibrary.com.]

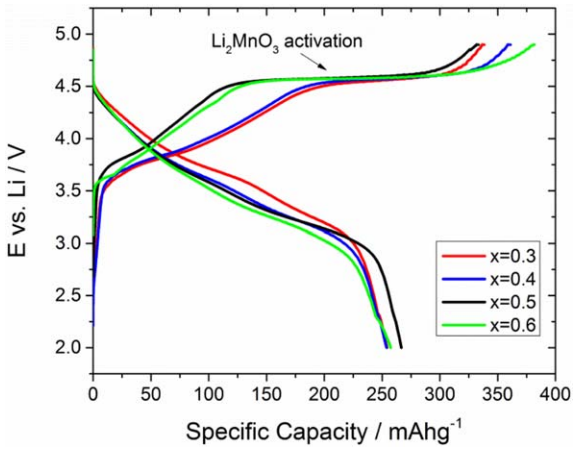

Figure 4. Initial charge-discharge voltage profile *vs.* capacity of $\text{Li}/x\text{Li}_2\text{MnO}_3\cdot(1\text{-}x)\text{LiNi}_{0.5}\text{Mn}_{0.5}\text{O}_2$ $(0.3 \le x \le 0.6)$ half cells.

The current density was 11.5 mAg^{-1}, with a cut-off voltage between 2.0 and 4.9 V. [Color figure can be viewed in the online issue, which is available at wileyonlinelibrary.com.]

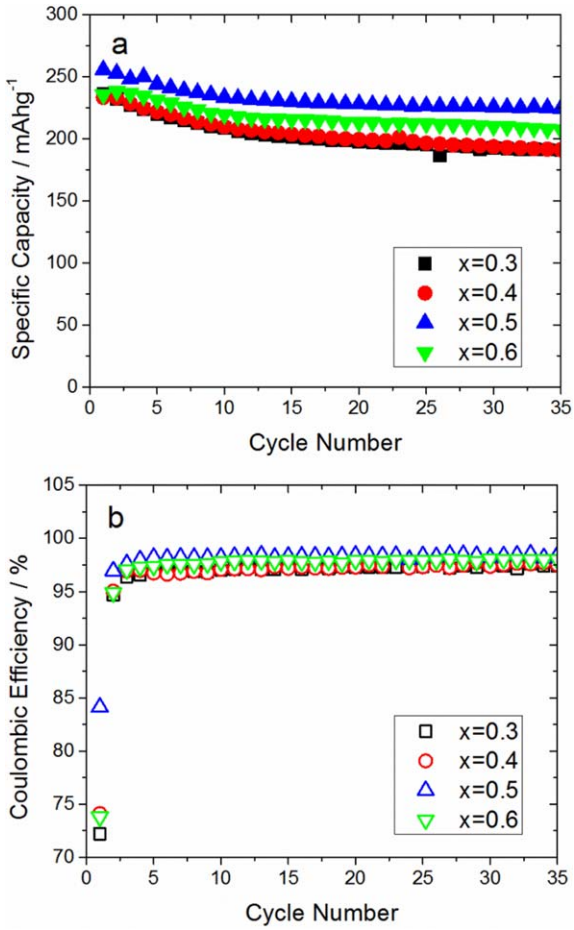

Figure 5. (a) Cycling performance of $\text{Li}/x\text{Li}_2\text{MnO}_3\cdot(1\text{-}x)\text{LiNi}_{0.5}\text{Mn}_{0.5}\text{O}_2$ $(0.3 \le x \le 0.6)$, (b) Coulombic efficiency of the cell at each cycle.

The current density was 23 mAg^{-1} in the voltage window between 2.0 and 4.8 V. [Color figure can be viewed in the online issue, which is available at wileyonlinelibrary.com.]

charge, owing to electrochemical activation of the Li_2MnO_3 component, as seen in Figure 6. The specific capacity (Q) with respect to the voltage (V) is given by $dQ/dV \approx \Delta Q/$

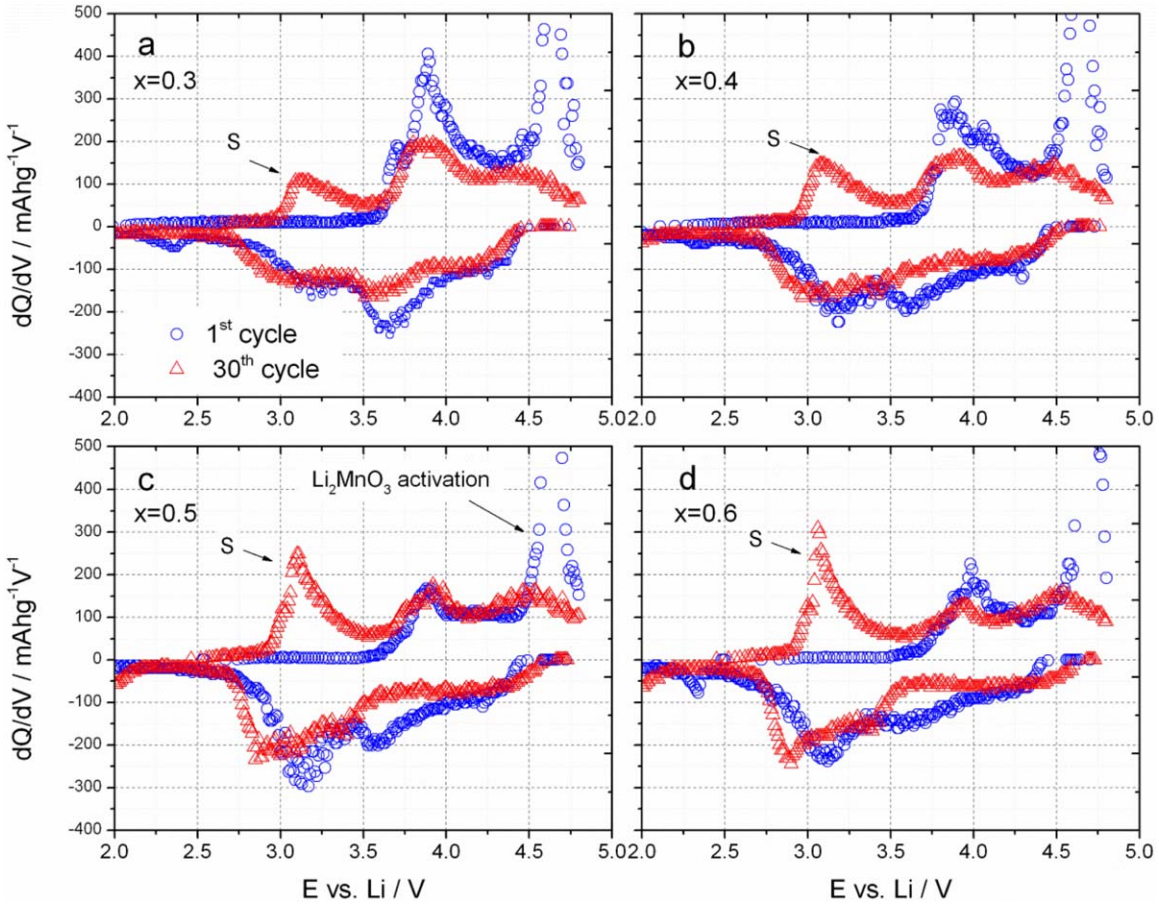

Figure 6. The dQ/dV curves of the Li/xLi$_2$MnO$_3$·(1-x)LiNi$_{0.5}$Mn$_{0.5}$O$_2$ ($0.3 \leq x \leq 0.6$) half cells for the initial cycle (open circle) and the 30th cycle (open triangle). "*S*" indicates the presence of the spinel phase.

[Color figure can be viewed in the online issue, which is available at wileyonlinelibrary.com.]

$\Delta V = i\Delta t/\Delta V$, where i is the current density (mAg^{-1}), t is time (s) and ΔV is normally 10 mV during the calculation. As x is increased, the Ni content in the structure decreases and the peak intensity between 3.5 V and 4.5 V from $Ni^{2+/3+/4+}$ redox reactions is broadening and diminishing on both first charge and discharge, consistent with our earlier discussion. In contrast, the peak near 3.2 V on the first discharge, which is due to the redox of $Mn^{3+/4+}$, increases with x, and is much more pronounced than the redox peak near 3.7 V for $x = 0.5$ or 0.6. This implies a high activity of Li_2MnO_3 component in these two composites. Consequently, a low-average working potential is attained. It is believed that at very high Mn concentration, a spinel phase may form during heat treatment.[47]

Nevertheless, the voltage profile of these composite materials appeared to be evolving during cycles, which is a function of the amount of Li_2MnO_3 content (x values), as seen on the dQ/dV curves at the 30th cycles (as compared to those of the first cycle). Two broad peaks near 3.1 V and 2.8 V, on charge and discharge, respectively, emerge, which are absent for the fresh cells. This suggests that a layered-spinel phase transition may have occurred over cycling, which changes the cell voltage profiles, depicted as a voltage decay phenomenon.[45] The spinel phase formation is facilitated by the migration of transition metal cations into the Li layer at a low Li content or at a high state-of-charge.[48,49] This spinel phase initially nucleates in the bulk and on the surface which slowly propagate throughout the grains of both $R\bar{3}m$ and $C2/m$ phases in the composite structure.[49] Therefore, the voltage continues to evolve over cycling. This phase transition is more severe at high Li and Mn concentrations (more Li_2MnO_3 phase), as the 3.1 V dQ/dV peak becomes more pronounced with x. In other words, a reduction in the Li_2MnO_3 ($C2/m$) phase reduces the voltage decay of the composite materials. Consequently, the composites need further optimization in the chemistry and morphology to enhance structure stability and to avoid an undesired phase transformation.

Conclusions

Nanostructured xLi$_2$MnO$_3$·(1-x)LiNi$_{0.5}$Mn$_{0.5}$O$_2$ ($0.3 \leq x \leq 0.6$) high-energy cathode materials were synthesized via a facile spray pyrolysis process. All the composite powders produced were spherical in shape and submicron in size. These materials overall adopted a rock-salt type structure ($R\bar{3}m$). A Li_2MnO_3-type phase was also observed for the composite material on the XRD pattern, and its intensity increased with x. All of the composites attained a capacity of ca. 250 mAhg^{-1} at the C/10 rates. 0.5Li$_2$MnO$_3$·0.5LiNi$_{0.5}$Mn$_{0.5}$O$_2$ attained the best cycling stability, while an increase in fraction of either the Li_2MnO_3 or $LiNi_{0.5}Mn_{0.5}O_2$ phase lead to a drop in cycleability. Despite the high-attainable capacities, a layered-spinel phase transition occurs, leading to voltage decay. The

voltage decay was more significant for the composites with higher Mn content (or Li_2MnO_3). In particular, $0.3Li_2MnO_3{\cdot}0.7LiNi_{0.5}Mn_{0.5}O_2$ from spray pyrolysis shows improved voltage stability and a higher discharge voltage due to the high Ni content. Further material optimization needs to be pursued to stabilize the structure, and, consequently, improve the cycle performance and voltage profile stability.

Acknowledgment

This work was supported in part by funding from the NSF under Grant No. 0928964. The authors thank Dr. Ilias Belharouak and Dr. Christopher Johnson at Argonne National Laboratory and Dr. Stephen Harris at General Motors (GM) for useful discussions. RLA and Washington University may receive income based on licensing of related technology by the University to X-tend Energy, LLC.

Literature Cited

1. Tarascon JM, Armand M. Issues and challenges facing rechargeable lithium batteries. *Nature*. 2001;414(6861):359–367.
2. Whittingham MS. Materials challenges facing electrical energy storage. *MRS Bulletin*. 2008;33:411–419.
3. Winter M, Besenhard JO, Spahr ME, Novak P. Insertion electrode materials for rechargeable lithium batteries. *Adv Mater*. 1998;10(10): 725–763.
4. Whittingham MS. Lithium batteries and cathode materials. *Chem Rev*. 2004;104(10):4271–4301.
5. Ammundsen B, Paulsen J. Novel lithium-ion cathode materials based on layered manganese oxides. *Adv Mater*. 2001;13(12-13):943–956.
6. Dahn JR, Vonsacken U, Michal CA. Structure and electrochemistry of $Li_{1\pm y}NiO_2$ and a new Li_2NiO_2 phase with the $Ni(OH)_2$ structure. *Solid State Ionics*. 1990;44(1-2):87–97.
7. Ozuku T, Makimura Y. Layered lithium insertion material of $LiNi_{1/2}Mn_{1/2}O_2$: A possible alternative to $LiCoO_2$ for advanced lithium-ion batteries. *Chem Lett*. 2001;8:744–745.
8. Kang SH, Kim J, Stoll ME, Abraham D, Sun YK, Amine K. Layered $Li(Ni_{0.5-x}Mn_{0.5-x}M'_{2x})O_2$ (M' = Co, Al, Ti; x = 0, 0.025) cathode materials for Li-ion rechargeable batteries. *J Power Sources*. 2002;112(1):41–48.
9. Reimers JN, Fuller EW, Rossen E, Dahn JR. Synthesis and electrochemical studies of $LiMnO_2$ prepared of low-temperatures. *J Electrochem Soc*. 1993;140(12):3396–3401.
10. Jang Y-I, Huang B, Wang H, Sadoway DR, Chiang YT. Electrochemical cycling-induced spinel formation in high-charge-capacity orthorhombic $LiMnO_2$. *J Electrochem Soc*. 1999;146(9):3217–3223.
11. Ohzuku T, Makimura Y. Layered lithium insertion material of $LiCo_{1/3}Ni_{1/3}Mn_{1/3}O_2$ for lithium-Ion batteries. *Chem Lett*. 2001; 30(7):642–643.
12. Lu ZH, MacNeil DD, Dahn JR. Layered cathode materials $Li[Ni_xLi_{(1/3-2x/3)}Mn_{(2/3-x/3)}]O_2$ for lithium-ion batteries. *Electrochem Solid State Lett*. 2001;4(11):A191–A194.
13. Lu ZH, Beaulieu LY, Donaberger RA, Thomas CL, Dahn JR. Synthesis, structure, and electrochemical behavior of $Li[Ni_xLi_{1/3-2x/3}Mn_{2/3-x/3}]O_2$. *J Electrochem Soc*. 2002;149(6):A778–A791.
14. Kang SH, Sun YK, Amine K. Electrochemical and ex situ X-ray study of $Li(Li_{0.2}Ni_{0.2}Mn_{0.6})O_2$ cathode material for Li secondary batteries. *Electrochem Solid State Lett*. 2003;6(9):A183–A186.
15. Johnson CS, Kim JS, Lefief C, Li N, Vaughey JT, Thackeray MM. The significance of the Li2MnO3 component in 'composite' $xLi_2MnO_3{\cdot}(1\text{-}x)LiMn_{0.5}Ni_{0.5}O_2$ electrodes. *Electrochem Commun*. 2004;6(10):1085–1091.
16. Shin SS, Sun YK, Amine K. Synthesis and electrochemical properties of $Li[Li_{(1-2x)/3}Ni_xMn_{(2-x)/3}]O_2$ as cathode materials for lithium secondary batteries. *J Power Sources*. 2002;112(2):634–638.
17. Deng H, Belharouak I, Amine K, Inventors. Nano-sized structured dense and spherical layered positive active materials provide high energy density and high rate capability electrodes in lithium-ion batteries. US patent US8277683 B2. May 22, 2009.
18. Croy JR, Kang SH, Balasubramanian M, Thackeray MM. Li_2MnO_3-based composite cathodes for lithium batteries: A novel synthesis approach and new structures. *Electrochem Commun*. 2011;13:1063–1066.
19. Thackeray MM, Kang SH, Johnson CS, Vaughey JT, Benedek R, Hackney SA. Li_2MnO_3-stabilized $LiMO_2$ (M = Mn, Ni, Co) electrodes for lithium-ion batteries. *J Mater Chem*. 2007;17(30):3112–3125.
20. Thackeray MM, Johnson CS, Vaughey JT, Li N, Hackney SA. Advances in manganese-oxide 'composite' electrodes for lithium-ion batteries. *J Mater Chem*. 2005;15(23):2257–2267.
21. Kim JS, Johnson CS, Vaughey JT, Thackeray MM, Hackney SA. Electrochemical and structural properties of $xLi_2M'O_3{\cdot}(1\text{-}x)LiMn_{0.5}Ni_{0.5}O_2$ eIectrodes for lithium batteries (M' = Ti, Mn, Zr; $0 \le x \le 0.3$). *Chem Mater*. 2004;16(10):1996–2006.
22. Thackeray MM, Johnson CS, Kim JS, Lefief C, Li N, Vaughey JT. The significance of the Li_2MnO_3 component in 'composite' $xLi_2MnO_3{\cdot}(1\text{-}x)LiMn_{0.5}Ni_{0.5}O_2$ electrodes. *Electrochem Commun*. 2004;6(10):1085–1091.
23. Johnson CS, Li NC, Lefief C, Thackeray MM. Anomalous capacity and cycling stability of $xLi_2MnO_3{\cdot}(1\text{-}x)LiMO_2$ electrodes (M= Mn, Ni, Co) in lithium batteries at 50°C. *Electrochem Commun*. 2007; 9(4):787–795.
24. Kang SH, Thackeray MM. Enhancing the rate capability of high capacity $xLi_2MnO_3{\cdot}(1\text{-}x)LiMO_2$ (M = Mn, Ni, Co) electrodes by Li-Ni-PO4 treatment. *Electrochem Commun*. 2009;11(4):748–751.
25. Deng HX, Belharouak I, Sun YK, Amine K. $Li_xNi_{0.25}Mn_{0.75}O_y$ ($0.5 \le x \le 2$, $2 \le y \le 2.75$) compounds for high-energy lithium-ion batteries. *J Mater Chem*. 2009;19(26):4510–4516.
26. Deng HX, Belharouak I, Cook RE, Wu HM, Sun YK, Amine K. Nanostructured lithium nickel manganese oxides for lithium-ion batteries. *J Electrochem Soc*. 2010;157(4):A447–A452.
27. Zhang XF, Axelbaum RL. Spray pyrolysis synthesis of mesoporous lithium-nickel-manganese-oxides for high energy Li-Ion batteries. *J Electrochem Soc*. 2012;159(6):A834–A842.
28. Ogihara T, Ogata N, Katayama K, Azuma Y, Mizutani N. Electrochemical properties of spherical, porous $LiMn_{2-x}Mg_xO_4$ powders prepared by ultrasonic spray pyrolysis. *Electrochem*. 2000;68(3):162–166.
29. Park SH, Yoon CS, Kang SG, Kim HS, Moon SI, Sun YK. Synthesis and structural characterization of layered $Li[Ni_{1/3}Co_{1/3}Mn_{1/3}]O_2$ cathode materials by ultrasonic spray pyrolysis method. *Electrochim Acta*. 2004;49(4):557–563.
30. Taniguchi I, Lim CK, Song D, Wakihara M. Particle morphology and electrochemical performances of spinel $LiMn_2O_4$ powders synthesized using ultrasonic spray pyrolysis method. *Solid State Ionics*. 2002;146:239–247.
31. Konarova M, Taniguchi I. Preparation of $LiFePO_4$/C composite powders by ultrasonic spray pyrolysis followed by heat treatment and their electrochemical properties. *Mater Res Bull*. 2008;43(12):3305–3317.
32. Matsuda K., Taniguchi I. Relationship between the electrochemical and particle properties of $LiMn_2O_4$ prepared by ultrasonic spray pyrolysis. *J Power Sources*. 2004;132:156–160.
33. Park SH, Oh SW, Myung ST, Kang YC, Sun YK. Effects of synthesis condition on $LiNi_{1/2}Mn_{3/2}O_4$ cathode material for prepared by ultrasonic spray pyrolysis method. *Solid State Ionics*. 2005;176(5-6): 481–486.
34. Wu HM, Tu JP, Yuan YF, Li Y, Zhao XB, Cao GS. Synthesis and electrochemical characteristics of spinel $LiMn_2O_4$ via a precipitation spray-drying process. *Mater Sci Eng B*. 2005;119:75–79.
35. Koo KY, Bin Parkw S. Preparation of iron phosphide particles from an aqueous solvent of oxygen-contained precursors using spray pyrolysis. *J Am Ceram Soc*. 2007;90(12):3767–3772.
36. Zhang X, Zheng H, Battaglia V, Axelbaum RL. Electrochemical performance of spinel $LiMn_2O_4$ cathode materials made by flame-assisted spray technology. *J Power Sources*. 2011;196(7):3640–3645.
37. Zhang X, Zheng H, Battaglia VS, Axelbaum RL. Flame synthesis of 5 V spinel-$LiNi_{0.5}Mn_{1.5}O_4$ cathode-materials for lithium-ion rechargeable-batteries. *Proc Comb Inst*. 2011;33(2):1867–1874.
38. Zhang XF, Lengyel M, Belharouak I, Axelbaum RL. Optimization of the Electrochemical Properties of $xLi_2MnO_3{\cdot}(1\text{-}x)LiMO_2$ Electrodes (M= Mn, Ni, Co) Prepared via Spray Pyrolysis Process. 2012 ECS Meeting - The Electrochemical Society. Seattle, WA; 2012.
39. Axelbaum RL, Zhang XF, Inventors; Washington University, assignee. Spray pyrolysis synthesis of mesoporous positive electrode materials for high energy lithium-ion batteries. US patent US20120282522 A1. 2012.
40. Son MY, Hong YJ, Choi SH, Kang YC. Effects of ratios of Li_2MnO_3 and $Li(Ni_{1/3}Mn_{1/3}Co_{1/3})O_2$ phases on the properties of composite cathode powders in spray pyrolysis. *Electrochim Acta*. 2013;103:110–118.

41. van Bommel A, Dahn JR. Synthesis of spherical and dense particles of the pure hydroxide phase $Ni_{1/3}Mn_{1/3}Co_{1/3}(OH)_2$. *J Electrochem Soc*. 2009;156(5):A362–A365.
42. Zhou F, Zhao XM, van Bommel A, Rowe AW, Dahn JR. Coprecipitation synthesis of $Ni_xMn_{1-x}(OH)_2$ mixed hydroxides. *Chem Mater*. 2010;22(3):1015–1021.
43. Lee ES, Huq A, Chang HY, Manthiram A. High-Voltage, high-energy layered-spinel composite cathodes with superior cycle life for lithium-ion batteries. *Chem Mater*. 2012;24(3):600–612.
44. Wang D, Belharouak I, Zhou GW, Amine K. Nanoarchitecture multi-structural cathode materials for high capacity lithium batteries. *Adv Funct Mater*. 2012.
45. Johnson CS, Li NC, Lefief C, Vaughey JT, Thackeray MM. Synthesis, characterization and electrochemistry of lithium battery electrodes: $xLi_2MnO_3{\cdot}(1\text{-}x)LiMn_{0.333}Ni_{0.333}Co_{0.333}O_2$ ($0 \leq x \leq 0.7$). *Chem Mater*. 2008;20(19):6095–6106.
46. Meng YS, Ceder G, Grey CP, et al. Cation ordering in layered O3 $Li[Ni_xLi_{1/3-2x/3}Mn_{2/3-x/3}]O_2$ ($0 \leq x \leq 1/2$) compounds. *Chem Mater*. 2005;17(9):2386–2394.
47. Rossouw MH, Thackeray MM. Lithium manganese oxides from Li_2MnO_3 for rechargeable lithium battery applications. *Mater Res Bull*. 1991;26(6):463–473.
48. Xu B, Fell CR, Chi MF, Meng YS. Identifying surface structural changes in layered Li-excess nickel manganese oxides in high voltage lithium ion batteries: A joint experimental and theoretical study. *Energ Environ Sci*. 2011;4(6):2223–2233.
49. Gu M, Belharouak I, Zheng JM, et al. Formation of the spinel phase in the layered composite cathode used in li-ion batteries. *Acs Nano*. 2013;7(1):760–767.

Manuscript received Aug. 5, 2013, and revision received Nov. 1, 2013.